

Inclusive electron-proton measurement prospects in the Electron-Ion Collider early science stage

Javier Jiménez-López ^{*1}, Stephen Maple ^{†2}, Paul R. Newman ^{‡3}, and Katarzyna Wichmann ^{§4}

¹*Departamento de Física Teórica, Universidad Complutense de Madrid, E-28040 Madrid, Spain*

^{2,3}*School of Physics and Astronomy, University of Birmingham, B15 2TT, UK*

⁴*Deutsches Elektronen-Synchrotron DESY, Germany*

DESY-25-164
November 2025

Abstract

We explore the potential for extracting proton structure functions, proton parton density functions (PDFs), and the strong coupling $\alpha_s(M_z^2)$, using early science data from the future Electron-Ion Collider (EIC), both standalone, and in combination with HERA data. Different scenarios are considered in which samples with modest luminosity are collected at either two or three EIC beam energy configurations. The Rosenbluth separation method is used to extract the proton structure functions F_2 and F_L from simulated data in a model-independent manner, showing that F_L can be extracted significantly more precisely with three centre of mass energies than with two, whilst also obtaining F_2 to higher precision than has been achieved previously. The inclusion of a third beam configuration is also beneficial in the extraction of the strong coupling $\alpha_s(M_z^2)$ that is obtainable with unprecedented experimental precision with the early EIC data. Additionally, the precision of the proton PDFs is improved when adding these data, especially for large values of Bjorken- x , for both two and three EIC beam energy configurations. These studies show that EIC data will already be a highly competitive probe of perturbative Quantum Chromodynamics within the first five years of data taking.

1 Introduction

The internal structure of the proton is an important topic in high-energy physics, offering insights into the composition and dynamics of strongly interacting matter. Central to these studies is the measurement of cross sections for Deep Inelastic Scattering (DIS) and thus of the proton structure functions, which in turn provide insight into the distributions of quarks and gluons in the nucleon [1]. The Hadron-Electron Ring Accelerator (HERA) was the first and, to date, the only high energy electron-proton colliding beam facility. It allowed measurements of inclusive Deep Inelastic Scattering (DIS) cross sections, and extraction of the structure functions F_2 , F_L and $xF_3^{\gamma Z}$ [2]. Among these, the generalised structure function, F_2 , is closely related to the quark density in the proton, whilst the gluon density can be obtained from the scaling violations of F_2 or from the longitudinal structure function F_L [3–9]. Knowledge of both the F_2 and F_L structure functions enables extractions of the photoabsorption ratio R , which corresponds to the cross section ratio for longitudinally to transversely polarised virtual photons interacting with the proton, such that

The extractions of F_L at HERA [10, 11] are limited by statistics and cover a restricted range at low values of the Bjorken variable x . The F_L structure function has also been measured at low Q^2 and large x by numerous

^{*}javiej09@ucm.es (Corresponding author)

[†]s.maple@bham.ac.uk

[‡]p.r.newman@bham.ac.uk

[§]katarzyna.wichmann@desy.de

fixed-target DIS experiments [12–18]. The Electron-Ion Collider [19] (EIC), which is expected to begin science operations at Brookhaven National Laboratory in the mid 2030s, promises to revolutionise our understanding of the internal structure of hadrons. Intended to operate at high luminosities and with a wide range of beam energy configurations, the EIC will provide the opportunity to extract the proton longitudinal structure function with unprecedented precision over a wide kinematic range in x and Q^2 [20].

The EIC project plan is divided such that the EIC science programme may commence before the full capabilities of the collider are realised. The “early science” period, is foreseen for the first five years of EIC operation and will provide access to a few selected centre-of-mass energies for electron-proton and electron-ion scattering data, with limited luminosities. At present, two different electron-proton beam energy configurations are anticipated for early science. In this study, we consider different approaches to extracting the F_2 and F_L structure functions using EIC early science data with two centre-of-mass energies, including extractions that combine HERA and EIC data. Additionally, we investigate the improvements that may be possible with the addition of a third centre-of-mass energy in the first five years. Further studies are conducted to evaluate the impact of EIC early science inclusive data on determinations of parton distribution functions (PDFs) and the strong coupling α_s .

2 EIC pseudo-data

The accelerator and detector designs for the EIC are currently undergoing intense development, but the overall specification in terms of beam energy ranges and instrumentation coverage and performance are already well-established [21]. The studies presented in this paper are based on simulated data points or ‘pseudo-data’ which are derived from that baseline configuration. Our approach to producing inclusive DIS EIC pseudo-data follows that of [20, 22], which in turn took binning schemes based on those in the ATHENA detector proposal [23]. The ATHENA collaboration has since merged with ECCE [24] to create the ePIC collaboration, which is now working towards a first EIC detector. While some specifics of the detectors have evolved, the overall expected kinematic range, kinematic variable resolutions and achievable experimental precision are largely independent of the detailed detector design and this study is thus applicable to any general purpose EIC experiment.

The EIC “early science” period, corresponding approximately to the first five years of data taking, is currently planned to include two distinct EIC ep beam energy settings, achieved via the scattering of 10 GeV electrons on 130 GeV or 250 GeV protons. The early science EIC will, however, be capable of operating with 5 GeV electron beams as well. When combined with the 130 GeV and 250 GeV proton beams this offers two additional beam energy configurations, $5 \times 130 \text{ GeV}^2$ and $5 \times 250 \text{ GeV}^2$. The $5 \times 250 \text{ GeV}^2$ and $10 \times 130 \text{ GeV}^2$ configurations are effectively degenerate in centre-of-mass energy. However, the $5 \times 130 \text{ GeV}^2$ beam setting offers a technically possible third point, which is additionally included in our studies. We therefore consider four scenarios: EIC pseudo-data only with either two or three beam energy settings, and HERA data combined with pseudo-data for either two or three EIC configurations. As summarised in Table 1, the EIC pseudo-data are thus produced for an integrated luminosity of 1 fb^{-1} , corresponding to conservative expectations for a few months of early science data collection, at three different centre-of-mass energies \sqrt{s} . Since we explore the possible extraction of the structure functions using EIC pseudo-data together with the final HERA inclusive DIS cross sections, the EIC Q^2 and x bin centres are chosen to match those of [2] for the e^+p scattering at four different centre-of-mass energies¹. For each beam configuration, the pseudo-data are produced at five logarithmically (but not evenly) spaced x values per decade over the inelasticity range $0.005 < y < 0.96$, matching the expected experimental resolutions [23]. The resolution of ePIC in Q^2 is expected to be significantly better than that of the HERA, so the HERA Q^2 binning is adopted.

The central values of the pseudo-data cross sections are obtained using NNLO theoretical predictions based on the HERAPDF 2.0 parton densities [2] within the xFitter framework [25–27], with the Q^2 evolution performed according to the NNLO DGLAP evolution equations [28–39]. The value for each data point is randomly smeared using samples from Gaussian distributions that reflect the assumed experimental uncertainties.

¹These bins do not correspond directly to the dedicated F_L measurements at HERA [10, 11] but to the general binning chosen for the combination of the H1 and ZEUS inclusive cross sections.

e -beam energy (GeV)	p -beam energy (GeV)	\sqrt{s} (GeV)	Integrated lumi (fb $^{-1}$)
10	250	100	1
10	130	72	1
5	130	51	1

Table 1: Beam energies, centre-of-mass energies and integrated luminosities assumed for the different EIC configurations considered for early science.

Taking into account that not all systematic uncertainties are known with certainty in this time several years before the commencement of early science operations, we consider the “conservative scenario” for the uncertainties introduced in [20]. It follows the considerations in [21], which were also adopted in the studies by the ATHENA collaboration, and subsequently used to study EIC collinear PDF sensitivities [22] and α_s measurements [40]. The data points are attributed a point-to-point uncorrelated systematic uncertainty of 1.9%, determined by the sum in quadrature of a conservative 1 % from radiative corrections, and 1.6 % from other effects such as bin migration, detector efficiency and charge symmetric background. A normalisation uncertainty of 3.4% is also included for each data set, which is not correlated between different beam energy configurations, such that the total systematic uncertainty attributed to each data point is 3.9 %. Here, the normalisation uncertainties comprise a 1.5 % contribution from the luminosity measurement, with the remaining 3 % arising from electron purity and detector efficiency effects.

The statistical uncertainties corresponding to 1 fb $^{-1}$ of integrated luminosity were confirmed in dedicated studies to be negligible compared to the systematic uncertainties, for all but the bins at the very largest x and Q^2 . This remains the case after including efficiency and resolution effects at a level that might be expected at the start of EIC operations.

3 Structure functions F_2 and F_L

The Rosenbluth separation technique used in the extraction of F_2 and F_L closely follows the method described in [20]. For $Q^2 \ll M_Z^2$ (mass of the Z boson squared), the inclusive cross section for Neutral Current (NC) DIS can be written in terms of F_2 and F_L as

$$\frac{d^2\sigma^{e^\pm p}}{dx dQ^2} = \frac{2\pi\alpha^2 Y_+}{xQ^4} \left[F_2(x, Q^2) - \frac{y^2}{Y_+} F_L(x, Q^2) \right] = \frac{2\pi\alpha^2 Y_+}{xQ^4} \sigma_r(x, Q^2, y) , \quad (1)$$

where α is the fine structure constant, $Y_+ = 1 + (1 - y)^2$, and σ_r is usually referred to as the reduced cross section.

Eq. 1 implies a linear relationship between the reduced cross section and y^2/Y_+ , which is a function only of the inelasticity of the process, and is adjustable at fixed x and Q^2 by changing the centre-of-mass energy and exploiting the relationship $Q^2 \simeq sxy$. Using measurements of σ_r at different s , the values of F_2 and F_L can thus be separately obtained in a model independent way as the free parameters of a linear fit. This Rosenbluth-type separation technique [41] has been applied to fixed target data and at HERA, and has also recently been used in a simulated extraction of the diffractive longitudinal structure function at the EIC [42]. For each (x, Q^2) , we thus apply a fit of the form

$$\sigma_r(x, Q^2, y) = F_2(x, Q^2) - \frac{y^2}{Y_+} F_L(x, Q^2) , \quad (2)$$

where $F_2(x, Q^2)$ and $F_L(x, Q^2)$ are free parameters, obtained through a χ^2 minimisation procedure as implemented in PYTHON using SciPy [43], with the uncertainties being obtained from variations of each parameter such that $\Delta\chi^2 = 1$.

The pseudo-data smearing procedure introduces randomness into the fit inputs, which is reflected in the results

as fluctuations in both the values and uncertainties of the extracted structure functions. The F_2 and F_L uncertainty results are therefore samples from distributions of possible outcomes which are often quite broad. In order to sample the distribution of possible uncertainty outcomes in a systematic way, we adopt the method introduced in [42] and used in [20], whereby the results are averaged over multiple replicas of the procedure. With a sufficiently large number of replicas (1000 is used by default), both the mean and the variance tend towards their expectation values for the simulated scenario. The average and variance are calculated as:

$$\bar{v} = \frac{S_1}{N}, \quad (\Delta v)^2 = \frac{S_2 - S_1^2/N}{N-1}, \quad (3)$$

where $S_n = \sum_{i=1}^N v_i^n$ and v_i is the value of structure function in the i -th MC sample.

3.1 Structure function results from combining HERA and two EIC beam configurations

We first study a potential extraction in which EIC pseudo-data at the two currently planned \sqrt{s} values are fitted together with HERA inclusive data at four different centre-of-mass energies, such that there are a total of six distinct beam energy configurations. Example results are shown for the F_2 and F_L structure functions and their uncertainties as obtained using this method in Fig. 1. For the HERA+EIC F_L measurements, points with absolute uncertainties larger than 0.5 are removed for visual clarity but all points for the F_2 measurements are shown. The HERA results and predictions from HERAPDF2.0 NNLO are also shown. For a given Q^2 bin, the HERA F_L measurements span a limited lever arm in x . With the inclusion of the EIC pseudo-data, model independent measurements of F_2 and F_L may be obtained for larger values of x , extending the F_L range by up to two orders of magnitude.

3.2 Structure function results from two EIC beam configurations alone

The extraction of the F_2 and F_L structure functions using the Rosenbluth method is usually based on three or more measurements at different centre-of-mass energies. The standard Rosenbluth separation procedure that was used in [42] and employed for other scenarios considered in this paper thus cannot be directly applied for the baseline assumption of two beam energy configurations in early EIC science. However, a simplified approach can be applied in which the slope and intercept of the line passing through the two measurements of σ_r when plotted against y^2/Y_+ are taken as directly corresponding to F_L and F_2 , respectively. The uncertainties on the structure functions can then be calculated using standard error propagation.

The expectation values and uncertainties of F_2 and F_L , obtained using only the two early science EIC beam energy configurations, are shown in Fig. 2. There are $\sim 15\%$ fewer F_L points with uncertainties of better than 0.5 (as chosen for plotting) in the EIC-only scenario compared to the HERA and EIC combined scenario. The impact of adding of a third EIC beam energy configuration, yielding a further \sqrt{s} value and a return to the χ^2 minimisation approach, is investigated in sections 3.3 and 3.4.

3.3 Kinematic coverage and precision for F_L with two or three EIC beam configurations

So far, we have considered only two distinct EIC ep beam energy settings, achieved via the scattering of 10 GeV electrons on 130 GeV or 250 GeV protons. Here we additionally present results when the third, lowest, EIC centre-of-mass energy, resulting from scattering of 5 GeV electrons with 130 GeV protons, is included in the analysis. Figure 3 shows absolute uncertainties on the simulated F_L measurements for the EIC-only scenarios, corresponding to two or three beam energy configurations, averaged over 1000 replicas. The difference in extraction methods and the number of data points used in the fits leads to very different uncertainties for the two and three-beam F_L results. This can be seen in Fig. 4 which shows the ratio of the absolute uncertainties for the three- to two-beam F_L results in the common kinematic region. The fits with the EIC-only data and

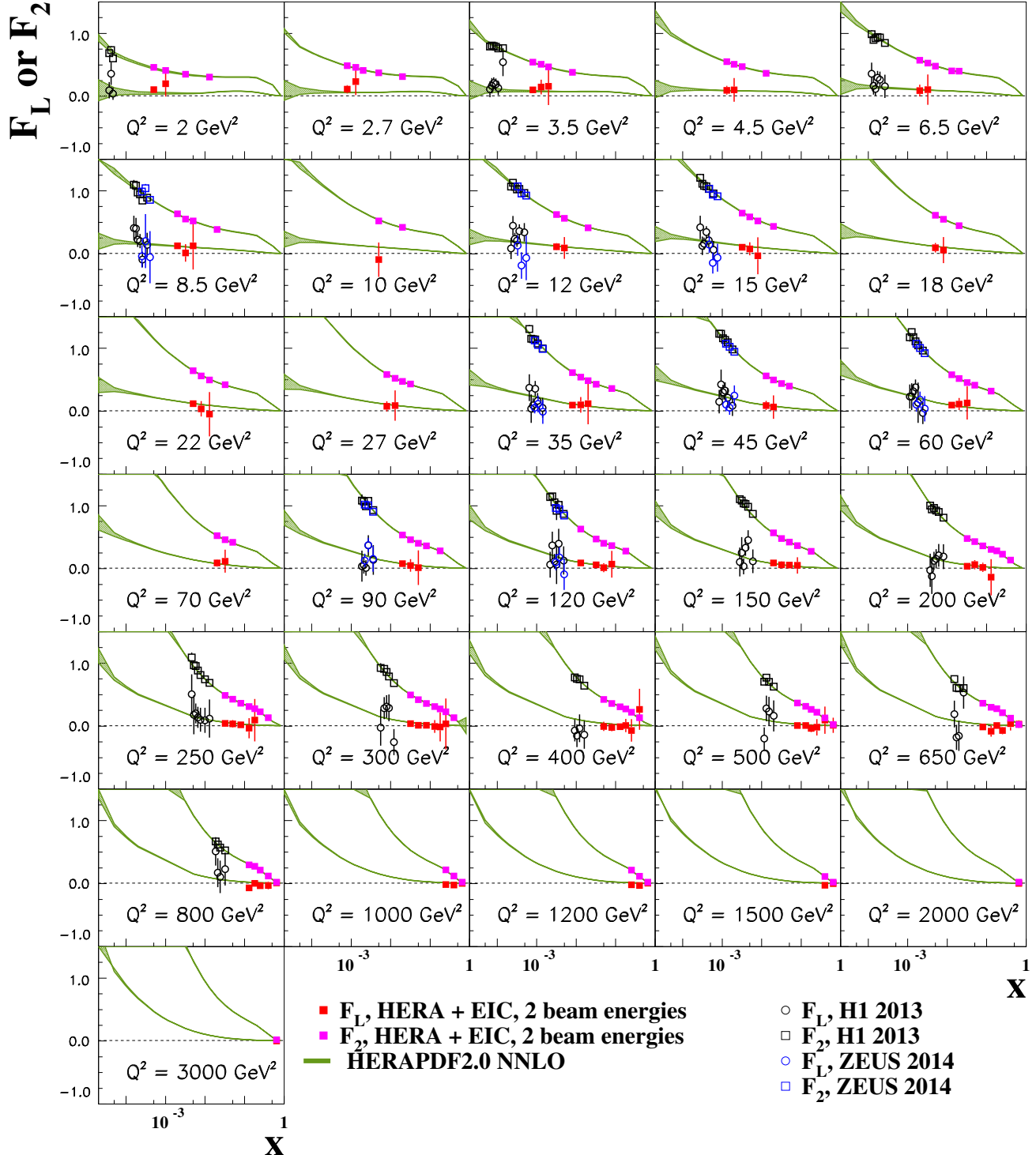


Figure 1: Simulated extractions of F_2 and F_L averaged over 1000 replicas for the fits with the HERA and EIC data, for two EIC beam energy configurations. (The two EIC centre-of-mass energies are 100 and 72 GeV.) The error bars on the points represent the total experimental uncertainties. For the HERA+EIC F_L measurements, points with absolute uncertainties larger than 0.5 are removed for visual clarity but all points for the F_2 measurements are shown.

three beam configurations give significantly more precise results for the F_L structure function compared to the two-beam scenario, the ratio typically falling between 10% and 20% and never exceeding 32%.

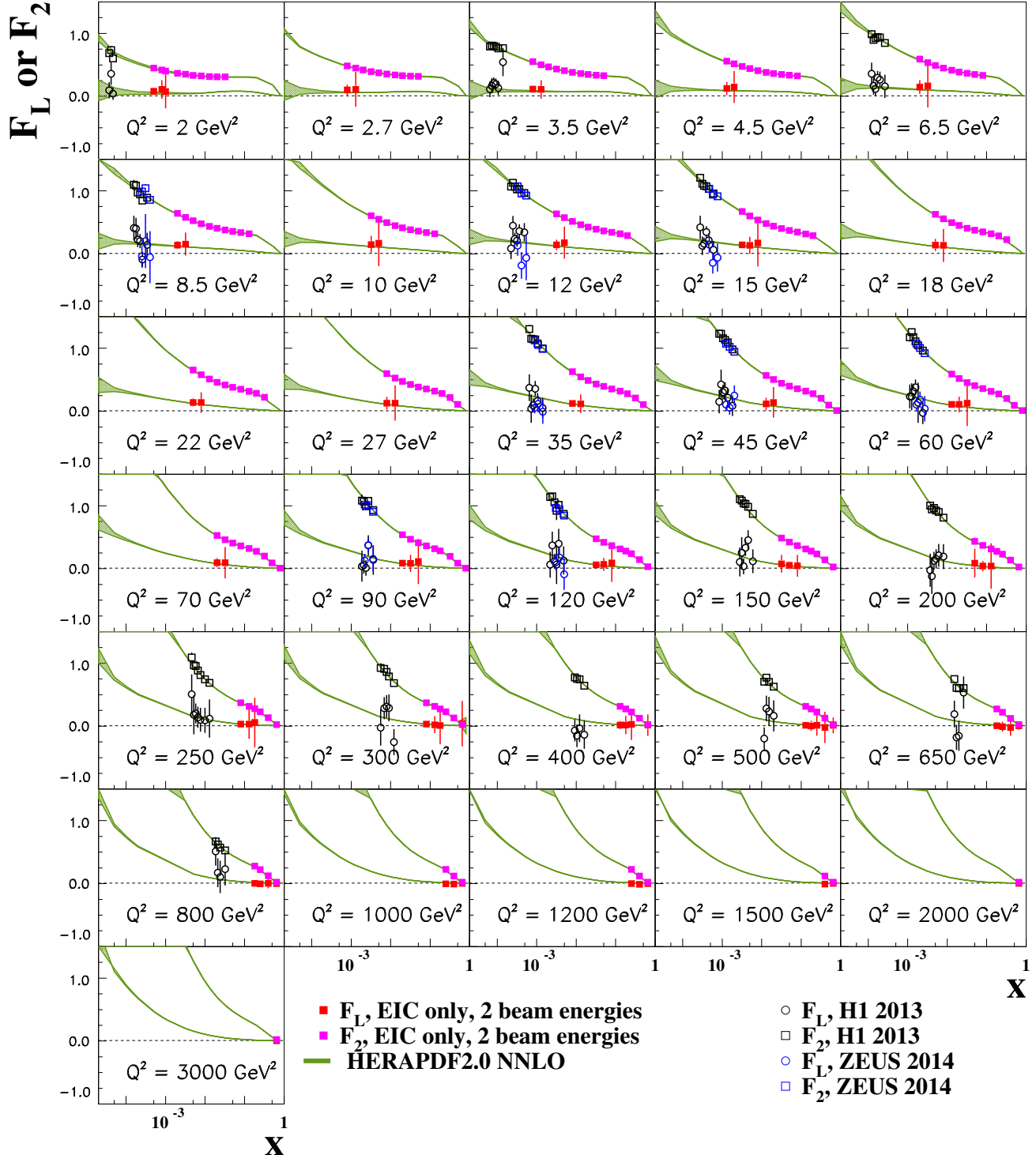


Figure 2: Simulated extractions of F_2 and F_L averaged over 1000 replicas for the fits with only two EIC beam energy configurations. (The two EIC centre-of-mass energies are 100 and 72 GeV.) The error bars on the points represent the total experimental uncertainties. For the EIC F_L measurements, points with absolute uncertainties larger than 0.5 are removed for visual clarity but all points for the F_2 measurements are shown.

Figure 5 shows absolute uncertainties on the simulated F_L measurements for HERA data combined with two or three EIC beam energy configurations, averaged over 1000 replicas. Here, for both two and three EIC beam energies, at least three data points are required to perform the Rosenbluth fits. As a result, the phase-space

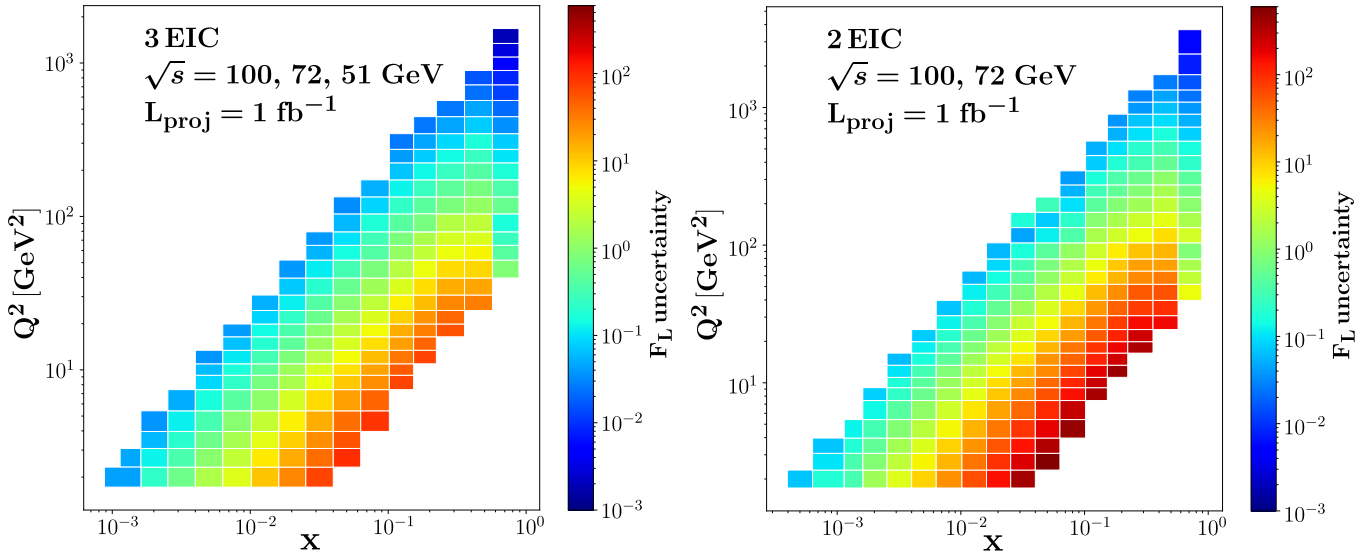


Figure 3: Absolute uncertainties on the simulated EIC-only F_L measurements averaged over 1000 replicas, corresponding to the three (left) and two (right) beam energy configurations, with the colours indicating the uncertainties. Note that different methods are applied in the two cases, with all three beam energies required to be available in the fits for the ‘3 EIC’ extraction and just two required for the ‘2 EIC’ case.

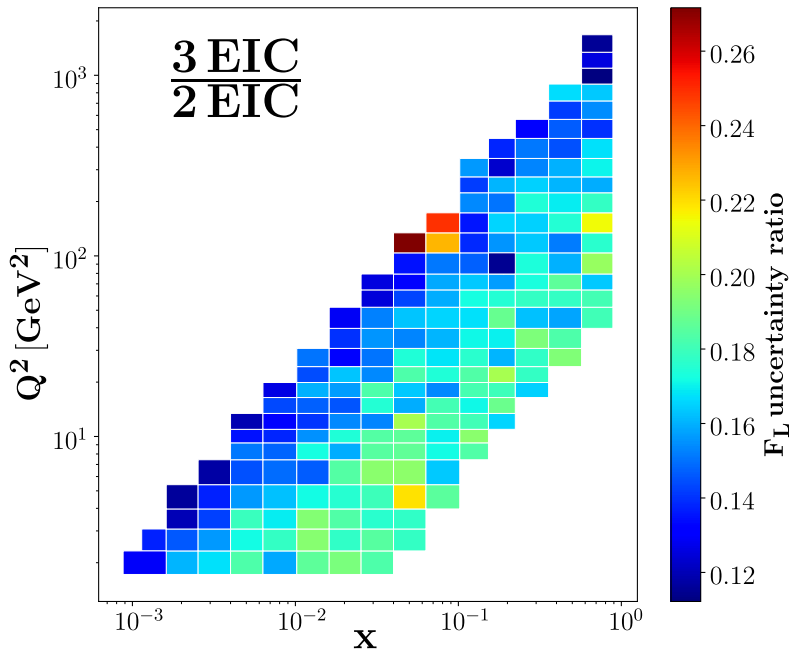


Figure 4: Ratio of absolute uncertainties on the simulated EIC F_L measurements for the three beam energy configuration over the two beam energy configuration, averaged over 1000 replicas. For the three beam energy configuration the EIC centre-of-mass energies are 100, 72 and 51 GeV. For the two beam energy configuration the EIC centre-of-mass energies are 100 and 72 GeV. All three beam energies are required in the fits for the ‘3 EIC’ extraction, whereas just two are required for the ‘2 EIC’ case.

for measurements using HERA and two EIC beam energies is considerably smaller than that for HERA and three EIC beam energies. Gaps in coverage appear in Fig. 6 where no HERA measurement is available for the chosen bin, due to the coarser binning of HERA measurements at large x and low Q^2 . Measurements in the three-beam scenario are more precise, though the difference is not as large as for the EIC-only case. This can be

seen in Fig. 6 which shows the ratio of the absolute uncertainties for the three- to two-beam F_L results for the fits with HERA + EIC data in the common kinematic region. The fits with the HERA and EIC data and three EIC beam configurations give significantly more precise results for the F_L structure function compared to the two-beam scenario, the ratio typically falling between 10% and 20% and never exceeding 30%. The precision of the F_L extraction depends on the y^2/Y_+ lever arm at a given x and Q^2 , which increases roughly as y_{\max}^2 , where y_{\max} is the largest y value included in the fit. With the inclusion of the lower energy EIC beam configuration, an additional high y data point becomes available, extending the y^2/Y_+ lever arm by a factor of $\sim 5 - 6$, which is reflected in the F_L uncertainties.

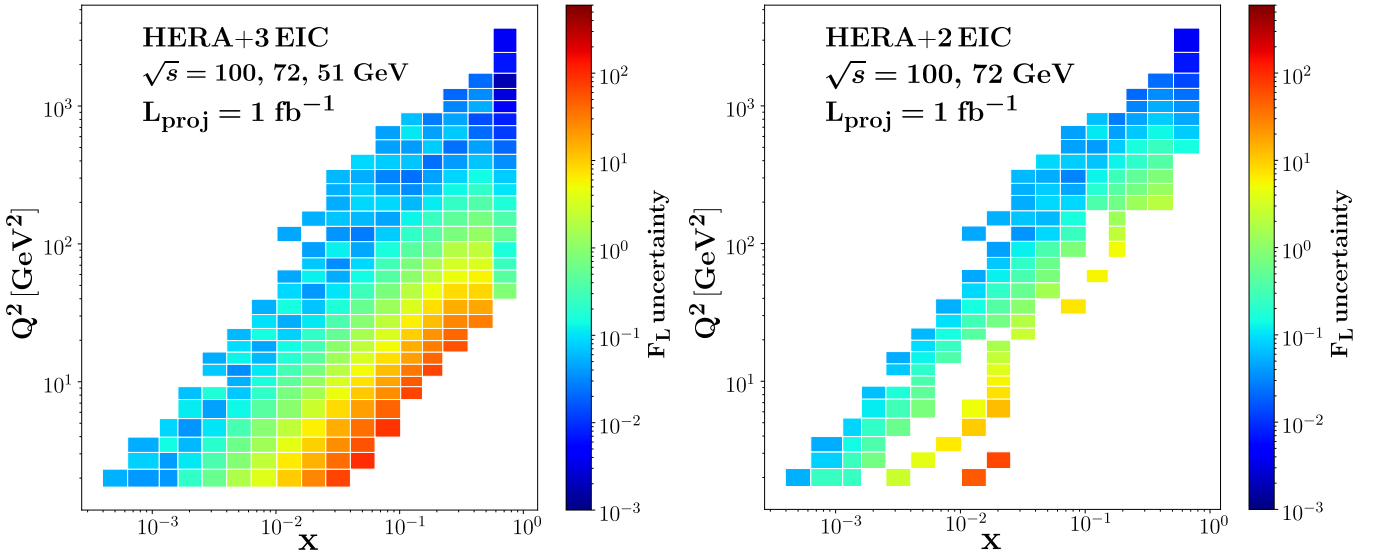


Figure 5: Absolute uncertainties on the simulated HERA+EIC F_L measurements averaged over 1000 replicas, corresponding to the three (left) and two (right) beam energy configurations, with the colours indicating the uncertainties. At least three data points are required for the Rosenbluth fits in both cases.

Figure 7 shows the phase-space accessible for the four measurement strategies discussed here, together with a selection of the previous structure function measurements.

3.4 Kinematic coverage and precision for F_2 with two or three EIC beam configurations

Figures 8 and 9 show absolute uncertainties on the simulated F_2 extractions, for EIC-only and HERA+EIC simulations, respectively, averaged over 1000 replicas. The kinematic region for the various scenarios is exactly the same as for the F_L extractions. The absolute uncertainties for F_2 are at the 10^{-2} level for most of the accessible kinematic plane. As expected, the three-beam scenario offers higher precision, for both EIC-only and HERA+EIC measurements.

In many HERA publications on inclusive cross sections when the F_2 structure function is extracted [27, 44–48], it is calculated from the reduced cross section σ_r using models to determine the size of the F_L contribution. In such publications, F_2 is either quoted without an uncertainty or the uncertainty is simply taken as a relative total uncertainty of the cross section. No model uncertainties are calculated. In contrast, the Rosenbluth separation method offers a completely model-independent extraction of F_2 . Here we investigate the improvements over the HERA extractions that can be obtained by adding EIC data and applying the Rosenbluth separation method. For all beam energies, the total uncertainties on the EIC cross sections are taken as 3.9% summed in quadrature with the statistical uncertainties (see Section 2).

Fig. 10 shows the ratio of F_2 uncertainties obtained using the model-independent Rosenbluth approach for various beam energy combinations, to those obtained using the HERA data only (i.e. with the fractional uncertainty taken directly from the reduced cross section). For the fits combining the HERA and EIC data

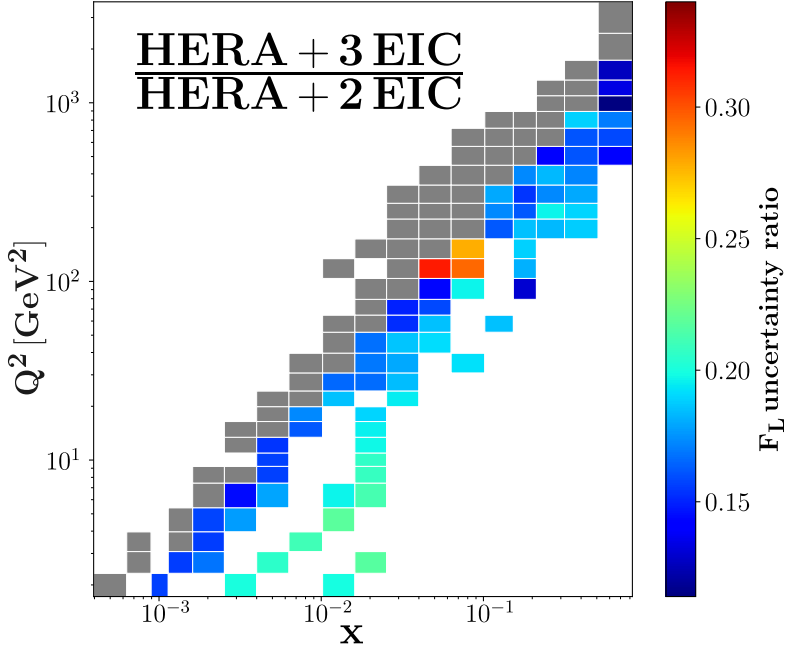


Figure 6: Ratio of absolute uncertainties on the simulated EIC F_L measurements for the three beam energy configuration over the two beam energy configuration, averaged over 1000 replicas. For the three beam energy configuration the EIC centre-of-mass energies are 100, 72 and 51 GeV. For the two beam energy configuration the EIC centre-of-mass energies are 100 and 72 GeV. At least three data points are required for the Rosenbluth fits in both cases. The grey boxes indicate cases where the ratio is exactly 1 by construction, because the same number of EIC points enter the Rosenbluth fits for the two- and three-beam scenarios.

and for the fits with EIC-only data with three centre-of-mass energies, the uncertainties obtained using the Rosenbluth separation are almost always lower than those from using HERA data alone. Exceptions only occur in cases where only one EIC point is used in the fit. For the EIC-only fits with three beam energies, all F_2 measurements are more precise than the HERA results in the regions of overlap, with improvements typically at the 20% level. Conversely, due to the difference in method, the scenario with EIC-only data and only two energies always leads to less precise results than those from HERA.

4 HERA+EIC collinear proton PDFs and strong coupling

Previous publications [40, 49] have shown that the full EIC DIS data will have a substantial impact on the precision of PDFs extracted in fits to DIS data only and on the strong coupling. Following these studies, similar analyses are performed here assuming 1 fb^{-1} of early science EIC data for the two- and three-beam configuration scenarios. The results presented in this section are obtained from global QCD fits at NNLO, performed in the HERAPDF2.0 framework [2] using xFitter, an open source QCD fit platform [25]. Fits with identical configurations are performed to HERA data only, corresponding to HERAPDF2.0 NNLO [2], and also with the additional inclusion of the simulated EIC early science NC DIS pseudo-data described in Section 2. To avoid regions that may be strongly affected by higher twist or resummation effects, a cut on the squared hadronic final state invariant mass, $W^2 = Q^2(1-x)/x > 10 \text{ GeV}^2$ is applied for all data. The central values of the PDFs with and without the EIC pseudo-data coincide by construction, so the uncertainties can be compared directly.

The impact of simulated early science EIC data in the two and three beam energy configurations on the NNLO collinear parton distributions of the proton is shown in Figures 11 and 12, with logarithmic and linear x scales, respectively, for the examples of the up-valence quarks and gluons. For low-to-mid x there is a modest

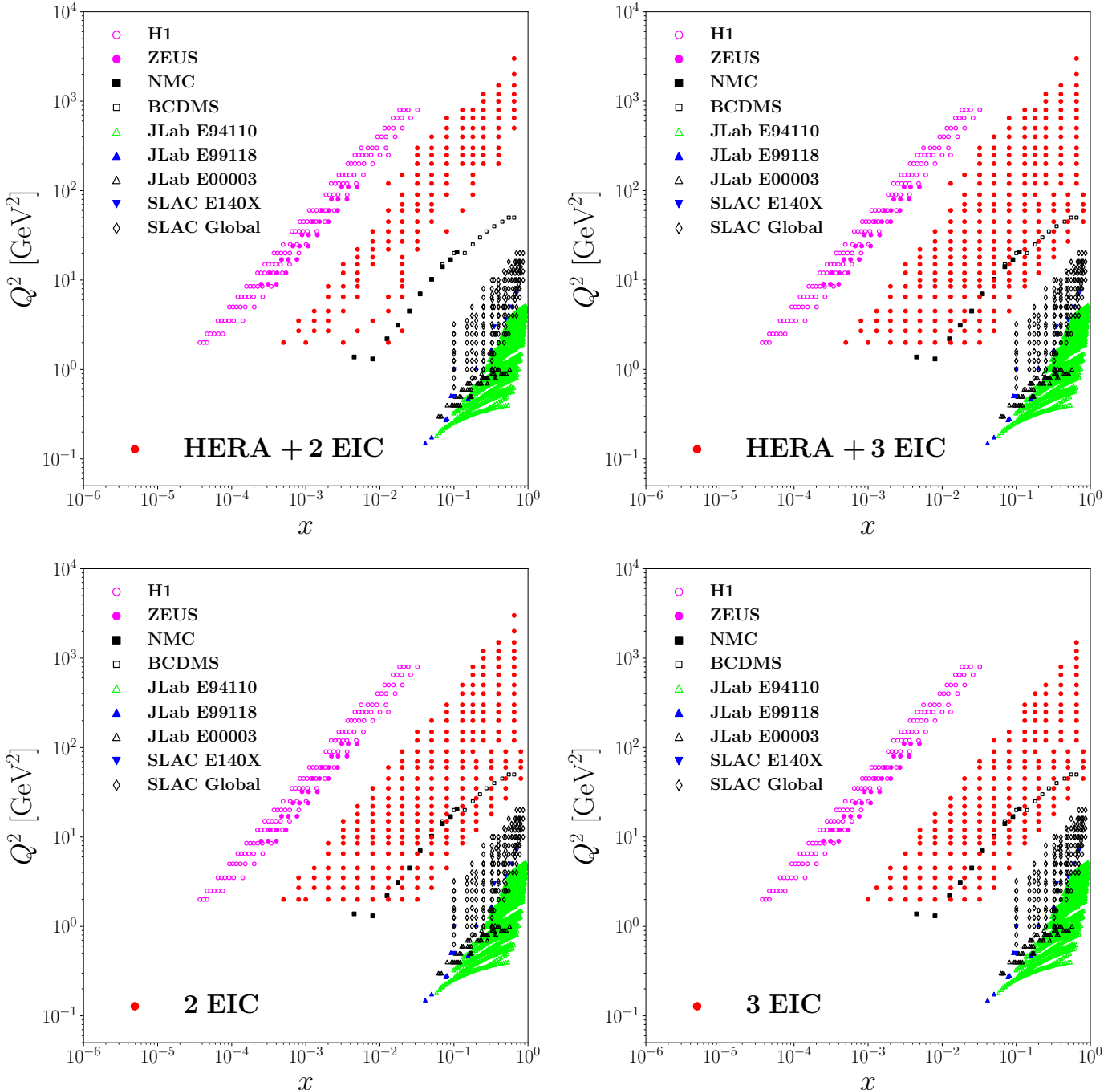


Figure 7: Kinematic coverage of world data for the proton longitudinal structure function, derived from figure 1 in [17], but with simulated EIC data added. The existing data shown are from H1 and ZEUS [10, 11], NMC [13], BCDMS [12], JLab [15, 17, 18] and SLAC [14, 16]. The EIC pseudo-data are shown for the fits with HERA + EIC data (top), and EIC data only (bottom), for the two (left) and three (right) beam scenarios. The EIC centre of mass energies are $\sqrt{s} = 100$ and 72 GeV for the two-beam case, with $\sqrt{s} = 51$ GeV added for the three-beam case. At least three \sqrt{s} values are required in the Rosenbluth fits in all cases except for the ‘2 EIC’ extraction, where both \sqrt{s} values are required.

improvement for both parton types with either EIC scenario. For intermediate and high $x > 0.1$, there is a somewhat larger improvement for the gluons and a very substantial improvement for up-valence quarks with the inclusion of early science EIC data. The down-valence quark distribution also exhibits a modest improvement, whilst only very small improvements are observed for the sea quark distributions (not shown). There is also very

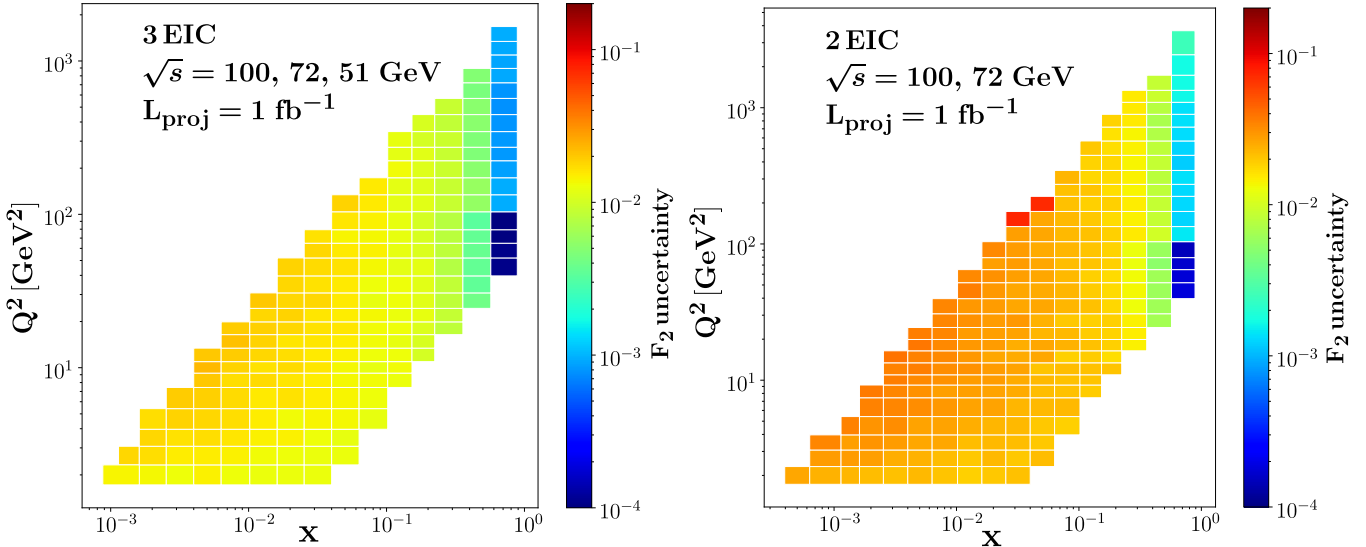


Figure 8: Absolute uncertainties on the simulated EIC-only F_2 measurements averaged over 1000 replicas, corresponding to the three (left) and two (right) beam energy configurations, with the colours indicating the absolute uncertainties.

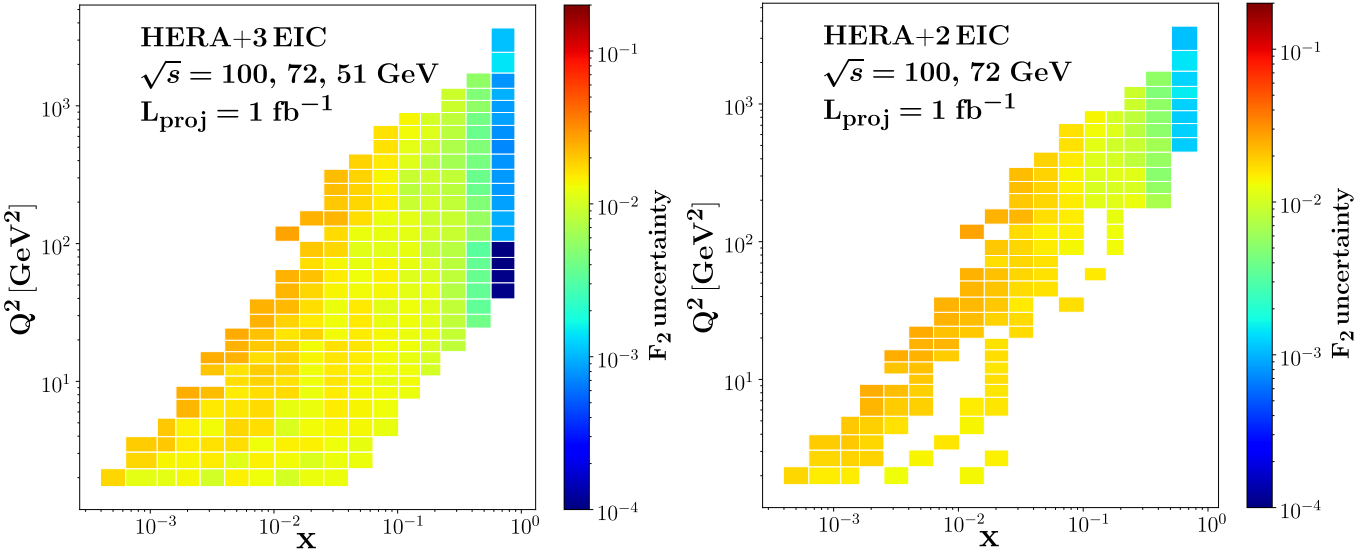


Figure 9: Absolute uncertainties on the simulated HERA+EIC F_2 measurements averaged over 1000 replicas, corresponding to the three (left) and two (right) beam energy configurations, with the colours indicating the absolute uncertainties.

little difference between the two and three EIC beam scenarios. When compared to the results assuming full longer-term EIC capabilities, including five different centre-of-mass energies and much larger integrated luminosities [49], the early science PDFs are clearly less precise for low-to-mid x and only slightly less precise for the large $x > 0.1$.

A similar procedure is used to extract the strong coupling α_s from the inclusive HERA and EIC data, using a simultaneous fit for PDFs and α_s , the only change being that the HERAPDF2.0 variant with input $\alpha_s(M_Z^2) = 0.116$ is used, for consistency with the HERAPDF2.0Jets NNLO [50] and a previous study of the EIC sensitivity to the strong coupling [40]. The procedure follows this previous publication closely. The results and uncertainties with and without the inclusion of EIC pseudo-data are shown in the form of a χ^2 scan as a function of $\alpha_s(M_Z^2)$

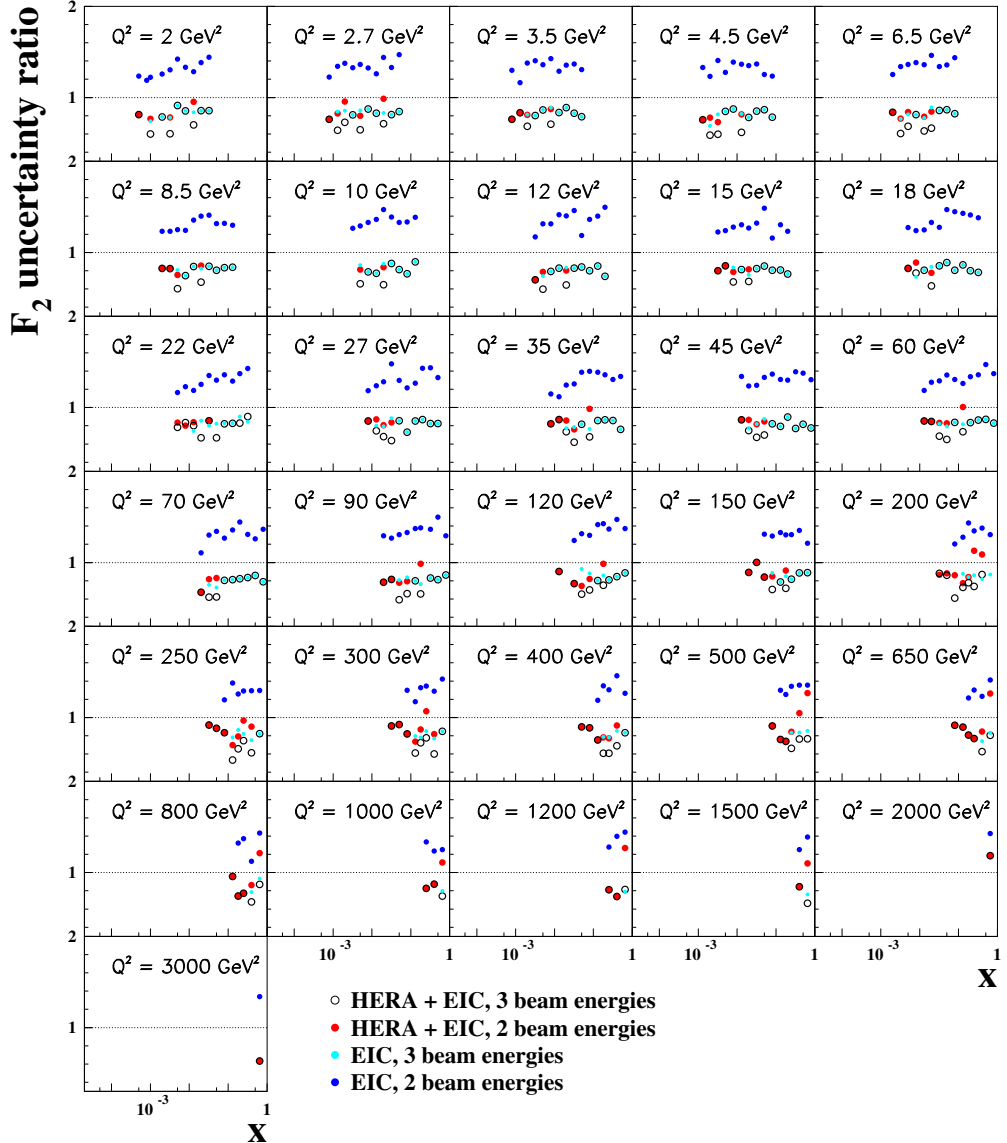


Figure 10: The ratio of F_2 uncertainties obtained using the model-independent Rosenbluth approach, to those obtained using HERA data only. Different symbols correspond to various beam energy combinations, for EIC-only and HERA+EIC fits. The beam settings are $\sqrt{s} = 100$ and 72 GeV for the two-beam case, with $\sqrt{s} = 51$ GeV added for the three-beam case.

in Fig. 13. Each point in the figure corresponds to a full QCD fit, with all 14 PDF parameters free and a fixed strong coupling value. The result without EIC pseudo-data is taken from [2]. The addition of the EIC early science data allows for a very precise extraction of the strong coupling.

The strong coupling extracted from the simultaneous fit for the PDFs and $\alpha_s(M_Z^2)$, using pseudo-data for the two energies of EIC early science together with the HERA inclusive data, is

$$\alpha_s(M_Z^2) = 0.1162 \pm 0.0008 \text{ (exp)}, \quad (4)$$

and that using the three energies of EIC pseudo-data is

$$\alpha_s(M_Z^2) = 0.1158 \pm 0.0006 \text{ (exp)}. \quad (5)$$

Here we quote only experimental uncertainties, since the model and parametrisation uncertainties are expected to be very small and the method for determining the theoretical uncertainties is uncertain (as discussed in [40]).

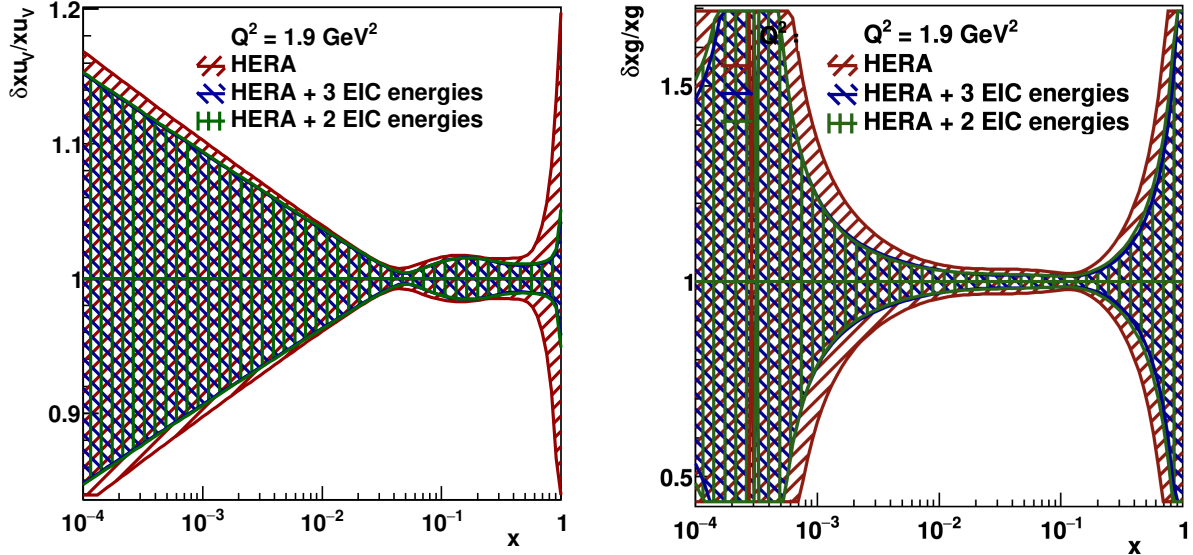


Figure 11: Impact of simulated EIC data on the NNLO collinear parton distributions of the proton (logarithmic x scale). The bands show relative experimental uncertainties for the up-valence and gluon distributions for $Q^2 = 1.9 \text{ GeV}^2$. The HERAPDF2.0NNLO total uncertainties (using HERA data alone) are compared with results in which simulated EIC data for different beam energy scenarios are also included in the HERAPDF2.0NNLO fitting framework. Beam settings are $\sqrt{s} = 100$ and 72 GeV for the two-beam case, with $\sqrt{s} = 51 \text{ GeV}$ added for the three-beam case.

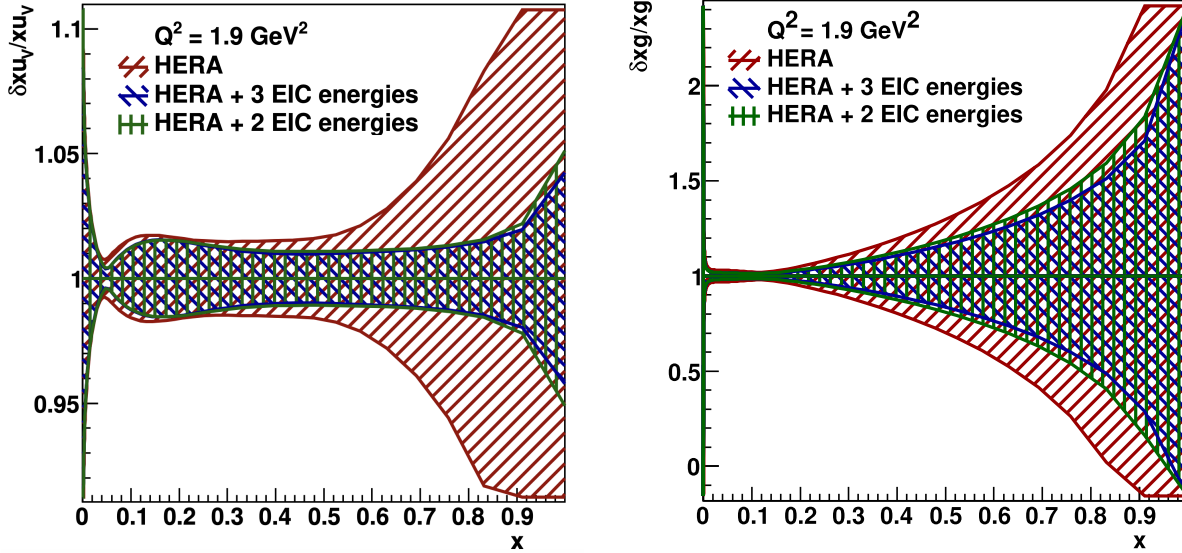


Figure 12: Impact of simulated EIC data on the NNLO collinear parton distributions of the proton (linear x scale). The bands show relative experimental uncertainties for the up-valence and gluon distributions for $Q^2 = 1.9 \text{ GeV}^2$. The HERAPDF2.0NNLO total uncertainties (using HERA data alone) are compared with results in which simulated EIC data for different beam energy scenarios are also included in the HERAPDF2.0NNLO fitting framework. Beam settings are $\sqrt{s} = 100$ and 72 GeV for the two-beam case, with $\sqrt{s} = 51 \text{ GeV}$ added for the three-beam case.

The $\alpha_s(M_Z^2)$ measurement is already very precise with two EIC beam configurations at the early science stage, reaching the level of the present world average or lattice QCD determinations. Adding the third (lower) energy improves these results by $\sim 25\%$. From the previous studies [40] the experimental uncertainty for five centre-of-mass energies assuming full long-term EIC capabilities in terms of luminosity and available beam energies is

HERA and EIC

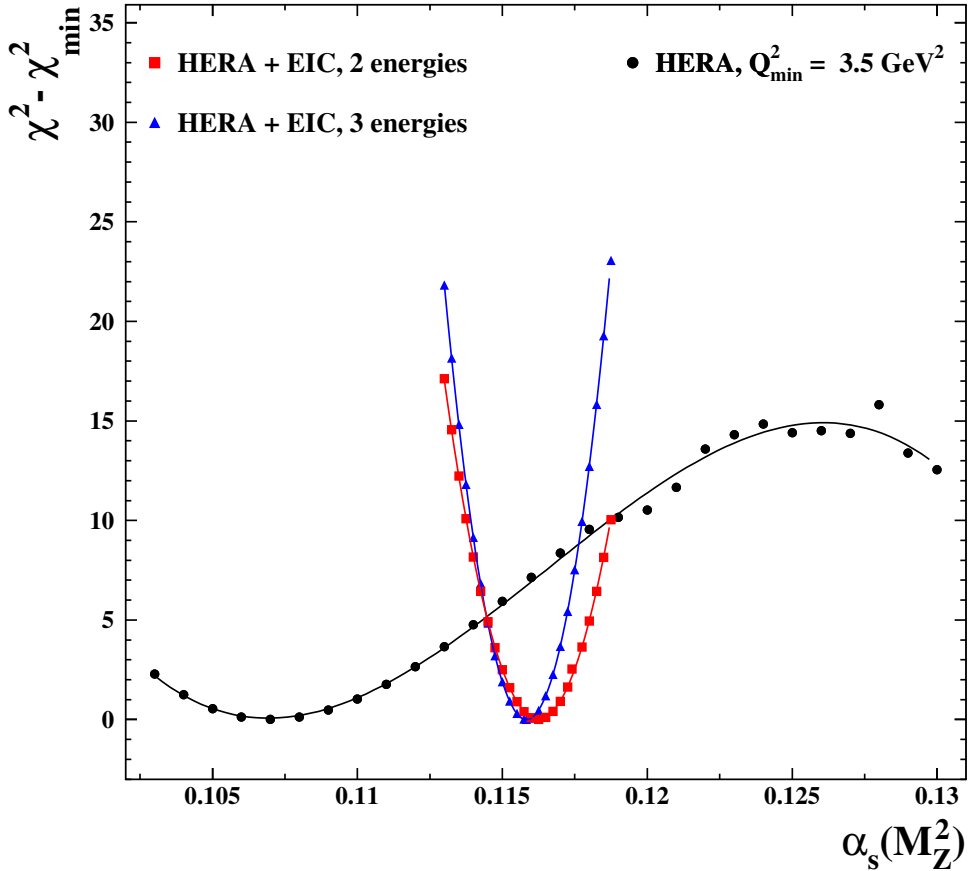


Figure 13: $\Delta\chi^2 = \chi^2 - \chi^2_{min}$ vs. $\alpha_s(M_Z^2)$ for the NNLO fits to HERA data on inclusive ep scattering only (black), and also with the addition of simulated EIC inclusive data for two (red) or three (blue) beam energies. The black full points are taken from [2].

expected to be ± 0.0004 .

5 Alternative Scenarios

The pseudo-data produced for the studies shown in this paper rely on assumptions for the available luminosity for each beam configuration, and also for the systematic precision that will be achieved for early science. Here, we briefly consider the impact of varying these assumptions on the results shown in this paper.

The pseudo-data were produced assuming integrated luminosity of 1 fb^{-1} in each beam configuration. On the other hand, recent projections indicate that the annual luminosity that could be delivered in the three early science beam configurations considered here of 5×130 , 10×130 , and $10 \times 250 \text{ GeV}^2$ would be 4.36 , 5.33 , and 9.18 fb^{-1} , respectively, in the so-called high divergence configuration. Assuming equivalent systematics to those used previously, and half year science periods with the luminosity for each configuration correspondingly scaled, no significant difference is observed in the precision of the extracted structure functions, or the uncertainties on the PDFs. For the α_s extraction, the increased luminosity improves the precision by about 15% and 20% for the two and three beam scenarios, respectively. This is a result of the improved uncertainties in the large x region, which is crucial for the precise extraction of the strong coupling, and is the only region where the statistical uncertainties dominate, thus benefitting the most from the increased luminosity.

During early science, it is likely that the electron-only method will be the main tool used in kinematic recon-

struction, as other methods that mix information from the scattered electron and the hadronic final state require a detailed understanding of the detector response to hadrons which may take time to achieve. The resolution achievable using the electron method degrades at low y as $\sim 1/y$, which in turn leads to larger systematic uncertainties, for example due to corrections for migrations between bins. We therefore consider a scenario where the point-to-point systematic uncertainty of 1.9% degrades as $1/y$ below a threshold value of $y_{\text{threshold}}$, where it is assumed that this effect dominates the systematic uncertainty. The point-to-point systematic uncertainty σ_{P2P} is therefore calculated as

$$\sigma_{\text{P2P}} = \begin{cases} \frac{y_{\text{threshold}}}{y} \times 1.9\%, & y < y_{\text{threshold}} \\ 1.9\%, & y > y_{\text{threshold}} \end{cases} \quad (6)$$

where $y_{\text{threshold}}$ is either 0.05 or 0.1. As before, little difference is found in the precision on the extracted structure functions, due to the lower impact of the low y points in a Rosenbluth fit compared with large y points. The only F_L points strongly affected by this change are those at the largest x for a given Q^2 , which already have very large uncertainties. No significant degradation in the precision of the PDFs is observed. The most impacted quantity is again α_s , due to its sensitivity to the large x data. With $y_{\text{threshold}} = 0.05$, a $\sim 50\%$ degradation is found, with $\delta\alpha_s = 0.0009$ for the three EIC energy scenario and $\delta\alpha_s = 0.0012$ for the two EIC energy case. For $y_{\text{threshold}} = 0.1$ this increases to $\delta\alpha_s = 0.0011$ and $\delta\alpha_s = 0.0015$ for the three and two EIC energy scenarios, respectively.

6 Summary

In this work, we have used simulated data to explore the potential of the Electron-Ion Collider (EIC) to measure the structure functions F_2 and F_L , as well as proton parton densities (PDFs) and the strong coupling $\alpha_s(M_Z^2)$, in the early EIC science stage (approximately the first five years). We have presented simulated model-independent measurements of the F_2 and F_L structure functions using a Rosenbluth fit method, for two and three EIC beam configuration scenarios, with and without the inclusion of the HERA data. Our studies show that the EIC will be able to measure the structure functions F_2 and F_L over a wide kinematic range in the first five years of operation, with a meaningful precision on F_L and improvements over the already very precise HERA data for F_2 . Our studies also show that, should a third ep run with a lower centre-of-mass energy be possible during the early science period, a factor of ~ 5 improvement to the F_L uncertainties may be achieved. In the PDF and $\alpha_s(M_Z^2)$ studies, the inclusion of EIC pseudo-data for the two beam configurations yields a clear improvement in the PDF uncertainties, and allows $\alpha_s(M_Z^2)$ to be constrained with world leading precision. Adding the third, lower centre-of-mass energy beam configuration does not have a strong impact on the PDF extraction. However it improves the $\alpha_s(M_Z^2)$ early science determination by $\sim 25\%$. The studies presented here clearly show that EIC data will already be a highly impactful probe of perturbative Quantum Chromodynamics within the first five years of data taking.

Acknowledgements

We are grateful to EIC and in particular ePIC collaboration colleagues whose efforts towards machine, detector and software development have enabled the creation of the simulated data used here. We also wish to thank many members of ePIC for valuable discussions and suggestions.

References

[1] R. Devenish and A. Cooper-Sarkar, *Deep inelastic scattering*. Oxford University Press, 2003.

- [2] H. Abramowicz *et al.*, “Combination of measurements of inclusive deep inelastic $e^\pm p$ scattering cross sections and QCD analysis of HERA data,” *Eur. Phys. J. C*, vol. 75, no. 12, p. 580, 2015.
- [3] S. Alekhin, J. Blümlein, S. Moch, and R. Placakyte, “Parton distribution functions, α_s , and heavy-quark masses for LHC Run II,” *Phys. Rev. D*, vol. 96, no. 1, p. 014011, 2017.
- [4] T.-J. Hou *et al.*, “New CTEQ global analysis of quantum chromodynamics with high-precision data from the LHC,” *Phys. Rev. D*, vol. 103, no. 1, p. 014013, 2021.
- [5] S. Bailey, T. Cridge, L. A. Harland-Lang, A. D. Martin, and R. S. Thorne, “Parton distributions from LHC, HERA, Tevatron and fixed target data: MSHT20 PDFs,” *Eur. Phys. J. C*, vol. 81, no. 4, p. 341, 2021.
- [6] R. D. Ball *et al.*, “The path to proton structure at 1% accuracy,” *Eur. Phys. J. C*, vol. 82, no. 5, p. 428, 2022.
- [7] A. M. Cooper-Sarkar, G. Ingelman, K. R. Long, R. G. Roberts, and D. H. Saxon, “Measurement of the longitudinal structure function and the small x gluon density of the proton,” *Z. Phys. C*, vol. 39, p. 281, 1988.
- [8] G. R. Boroun and B. Rezaei, “Analysis of the proton longitudinal structure function from the gluon distribution function,” *Eur. Phys. J. C*, vol. 72, p. 2221, 2012.
- [9] E. B. Zijlstra and W. L. van Neerven, “Order α_s^2 QCD corrections to the deep inelastic proton structure functions F_2 and $F(L)$,” *Nucl. Phys. B*, vol. 383, pp. 525–574, 1992.
- [10] V. Andreev *et al.*, “Measurement of inclusive ep cross sections at high Q^2 at $\sqrt{s} = 225$ and 252 GeV and of the longitudinal proton structure function F_L at HERA,” *Eur. Phys. J. C*, vol. 74, no. 4, p. 2814, 2014.
- [11] H. Abramowicz *et al.*, “Deep inelastic cross-section measurements at large y with the ZEUS detector at HERA,” *Phys. Rev. D*, vol. 90, no. 7, p. 072002, 2014.
- [12] A. Benvenuti *et al.*, “A high statistics measurement of the proton structure functions $F_2(x, Q^2)$ and R from deep inelastic muon scattering at high Q^2 ,” *Physics Letters B*, vol. 223, no. 3, pp. 485–489, 1989.
- [13] M. Arneodo *et al.*, “Measurement of the proton and deuteron structure functions, F_2^p and F_2^d , and of the ratio σ_L/σ_T ,” *Nuclear Physics B*, vol. 483, no. 1, pp. 3–43, 1997.
- [14] L. H. Tao *et al.*, “Precision measurement of $R = \sigma_L/\sigma_T$ on hydrogen, deuterium and beryllium targets in deep inelastic electron scattering,” *Z. Phys. C*, vol. 70, pp. 387–390, 1996.
- [15] V. Tvaskis *et al.*, “Longitudinal-transverse separations of structure functions at low Q^2 for hydrogen and deuterium,” *Phys. Rev. Lett.*, vol. 98, p. 142301, 2007.
- [16] L. W. Whitlow *et al.*, “Precise measurements of the proton and deuteron structure functions from a global analysis of the SLAC deep inelastic electron scattering cross-sections,” *Phys. Lett. B*, vol. 282, pp. 475–482, 1992.
- [17] V. Tvaskis *et al.*, “Measurements of the separated longitudinal structure function F_L from hydrogen and deuterium targets at low Q^2 ,” *Phys. Rev. C*, vol. 97, p. 045204, 2018.
- [18] Y. Liang *et al.*, “Measurement of $R = \sigma_L/\sigma_T$ and the separated longitudinal and transverse structure functions in the nucleon-resonance region,” *Phys. Rev. C*, vol. 105, no. 6, p. 065205, 2022.
- [19] A. Accardi *et al.*, “Electron Ion Collider: The Next QCD Frontier: Understanding the glue that binds us all,” *Eur. Phys. J. A*, vol. 52, no. 9, p. 268, 2016.
- [20] J. Jiménez-López, P. R. Newman, and K. Wichmann, “Prospects for measurements of the longitudinal proton structure function F_L at the Electron Ion Collider,” *Phys. Rev. D*, vol. 111, no. 5, p. 056014, 2025.

[21] R. Abdul Khalek *et al.*, “Science Requirements and Detector Concepts for the Electron-Ion Collider: EIC Yellow Report,” *Nucl. Phys. A*, vol. 1026, p. 122447, 2022.

[22] N. Armesto *et al.*, “Impact of inclusive electron ion collider data on collinear parton distributions,” *Phys. Rev. D*, vol. 109, no. 5, p. 054019, 2024.

[23] J. Adam *et al.*, “ATHENA detector proposal — a totally hermetic electron nucleus apparatus proposed for IP6 at the Electron-Ion Collider,” *JINST*, vol. 17, no. 10, p. P10019, 2022.

[24] J.K. Adkins *et al.*, “Design of the ECCE Detector for the Electron Ion Collider.” [physics.ins-det/2209.02580]. JLAB-PHY-24-4124, 2022.

[25] S. Alekhin *et al.*, “HERAFitter,” *Eur. Phys. J. C*, vol. 75, no. 7, p. 304, 2015.

[26] F. D. Aaron *et al.*, “Combined measurement and QCD analysis of the inclusive $e^\pm p$ scattering cross sections at HERA,” *JHEP*, vol. 01, p. 109, 2010.

[27] F. D. Aaron *et al.*, “A Precision Measurement of the Inclusive ep Scattering Cross Section at HERA,” *Eur. Phys. J. C*, vol. 64, pp. 561–587, 2009.

[28] V. N. Gribov and L. N. Lipatov, “Deep inelastic ep scattering in perturbation theory,” *Sov. J. Nucl. Phys.*, vol. 15, pp. 438–450, 1972.

[29] V. N. Gribov and L. N. Lipatov, “ e^+e^- pair annihilation and deep inelastic $e p$ scattering in perturbation theory,” *Sov. J. Nucl. Phys.*, vol. 15, pp. 675–684, 1972.

[30] L. N. Lipatov, “The parton model and perturbation theory,” *Yad. Fiz.*, vol. 20, pp. 181–198, 1974.

[31] Y. L. Dokshitzer, “Calculation of the structure functions for deep inelastic scattering and e^+e^- annihilation by perturbation theory in Quantum Chromodynamics.,” *Sov. Phys. JETP*, vol. 46, pp. 641–653, 1977.

[32] G. Altarelli and G. Parisi, “Asymptotic freedom in parton language,” *Nucl. Phys. B*, vol. 126, pp. 298–318, 1977.

[33] S. Moch, J. A. M. Vermaseren, and A. Vogt, “The three loop splitting functions in QCD: The nonsinglet case,” *Nucl. Phys. B*, vol. 688, pp. 101–134, 2004.

[34] A. Vogt, S. Moch, and J. A. M. Vermaseren, “The three-loop splitting functions in QCD: The singlet case,” *Nucl. Phys. B*, vol. 691, pp. 129–181, 2004.

[35] A. A. Almasy, S. Moch, and A. Vogt, “On the next-to-next-to-leading Order evolution of flavour-singlet fragmentation functions,” *Nucl. Phys. B*, vol. 854, pp. 133–152, 2012.

[36] A. Mitov, S. Moch, and A. Vogt, “Next-to-next-to-leading order evolution of non-singlet fragmentation functions,” *Phys. Lett. B*, vol. 638, pp. 61–67, 2006.

[37] J. Blümlein, P. Marquard, C. Schneider, and K. Schönwald, “The three-loop unpolarized and polarized non-singlet anomalous dimensions from off shell operator matrix elements,” *Nucl. Phys. B*, vol. 971, p. 115542, 2021.

[38] J. Ablinger, A. Behring, J. Blümlein, A. De Freitas, A. von Manteuffel, C. Schneider, and K. Schönwald, “The three-loop single-mass heavy flavor corrections to deep-inelastic scattering,” *PoS*, vol. LL2024, p. 047, 2024.

[39] J. Ablinger, A. Behring, J. Blümlein, A. De Freitas, A. von Manteuffel, C. Schneider, and K. Schönwald, “The three-loop single-mass heavy-flavor corrections to the structure functions $F_2(x, Q^2)$ and $g_1(x, Q^2)$,” 9 2025.

[40] S. Cerci *et al.*, “Extraction of the strong coupling with HERA and EIC inclusive data,” *Eur. Phys. J. C*, vol. 83, no. 11, p. 1011, 2023.

[41] M. N. Rosenbluth, “High energy elastic scattering of electrons on protons,” *Phys. Rev.*, vol. 79, pp. 615–619, 1950.

[42] N. Armesto, P. R. Newman, W. Słomiński, and A. M. Staśto, “Diffractive longitudinal structure function at the Electron Ion Collider,” *Phys. Rev. D*, vol. 105, no. 7, p. 074006, 2022.

[43] P. Virtanen *et al.*, “SciPy 1.0—Fundamental algorithms for scientific computing in Python,” *Nature Meth.*, vol. 17, p. 261, 2020.

[44] C. Adloff *et al.*, “Measurement of neutral and charged current cross-sections in positron proton collisions at large momentum transfer,” *Eur. Phys. J. C*, vol. 13, pp. 609–639, 2000.

[45] C. Adloff *et al.*, “Measurement of neutral and charged current cross-sections in electron - proton collisions at high Q^2 ,” *Eur. Phys. J. C*, vol. 19, pp. 269–288, 2001.

[46] C. Adloff *et al.*, “Measurement and QCD analysis of neutral and charged current cross-sections at HERA,” *Eur. Phys. J. C*, vol. 30, pp. 1–32, 2003.

[47] F. D. Aaron *et al.*, “Measurement of the Inclusive ep Scattering Cross Section at Low Q^2 and x at HERA,” *Eur. Phys. J. C*, vol. 63, pp. 625–678, 2009.

[48] S. Chekanov *et al.*, “Measurement of the neutral current cross-section and $F(2)$ structure function for deep inelastic $e + p$ scattering at HERA,” *Eur. Phys. J. C*, vol. 21, pp. 443–471, 2001.

[49] N. Armesto, T. Cridge, F. Giuli, L. Harland-Lang, P. Newman, B. Schmookler, R. Thorne, and K. Wichmann, “Impact of inclusive electron ion collider data on collinear parton distributions,” *Physical Review D*, vol. 109, no. 5, p. 054019, 2024.

[50] I. Abt *et al.*, “Impact of jet-production data on the next-to-next-to-leading-order determination of HERAPDF2.0 parton distributions,” *Eur. Phys. J. C*, vol. 82, no. 3, p. 243, 2022.